Supporting Information

In situ generated 2,5-pyrazinedicarboxylate and oxalate ligands leading to a Eu-MOF for selective capture of C_2H_2 from C_2H_2/CO_2

*Fenglan Liang,[a] Deyun Ma,[*b] Liang Qin,[b] Qiuqun Yu,[b] Jing Chen,[b] Rongxi Liang,[b] Changheng Zhong,[b] Huanzong Liao,[b] Zhiyi Peng,[b]*

[a] College of Life Science, Zhaoqing University, Zhaoqing, 526061, PR China.

[b] School of Food and Pharmaceutical Engineering, Zhaoqing University, Zhaoqing 526061, China. E-mail: mady@zqu.edu.cn.

Experimental

5-methylpyrazine-2-carboxylic acid and $Eu(NO_3)_3·6(H_2O)$ were purchased from Aladdin company.

Synthesis of $\{[Eu_2(pzdc)(ox)_2(H_2O)_4]·5H_2O\}_n$ ***(1)***: To an aqueous solution (10 mL) of dilute nitric acid (0.16 mL), 5-methylpyrazine-2-carboxylic acid (0.138 g, 1 mmol), and $Eu(NO_3)_3·6(H_2O)$ (0.223 g, 0.5 mmol) were added. The mixed solution was sealed in a Teflon reactor (23 mL) and kept at 150 °C for 72 h. Finally, yellow crystals were collected (yield: 58%). Anal. Calcd for $C_{10}H_{20}Eu_2N_2O_{21}$ (**1**): C, 14.8; H, 2.5. N, 3.4. Found: C, 14.6; H, 2.3; N, 3.6. IR (KBr pellet) (cm^{-1}): 3450(s), 1589(vs), 1482(m), 1383(s), 1307(s), 1182(m), 1043(m), 839(m), 773(m), 517(w), 473(w), (Fig. S1).

X-ray crystal structural determination: The crystal data of **1** were collected on a Bruker Apex II CCD diffractometer at 50 kV and 30 mA with MoKα radiation (λ = 0.71073 Å). The crystal was kept at 150 K during the measurement. Data collection and reduction were performed using the APEX II software.[1a] The crystal structure of **1** was solved using direct methods followed by least-squares on F^2 using SHELXTL.[1b] Non-hydrogen atoms were refined with independent anisotropic displacement parameters and hydrogen atoms attached to carbon and oxygen were placed in geometrically idealized positions and refined using the riding model. The TOPOS software was used to topologically analyze **1**.[1c-d] The more detail information is listed in the CIF file. Crystal data, as well as detail of data collection and refinement are shown in Table S1. Selected bond lengths and bond angles of **1** are summarized in Table S2.

Material characterization: Elemental analyses were performed on a Vario EL III Elemental Analyzer. IR spectra were obtained on a Shimadzu IR-440 spectrometer in the range of 4000-400 cm^{-1} (KBr disk). Thermogravimetric analysis (TGA) was carried out on an automatic simultaneous thermal analyzer (DTG-60, Shimadzu)

under N_2 aEuosphere from 25 to 800 °C with a heating rate of 10 °C/min. Powder X-ray diffraction patterns (PXRD) were measured by using a Bruker AXS D8-Advance diffractometer with Cu-Kα (λ = 1.5418 Å) radiation. The simulated pattern was produced using the Mercury V1.4 program and single-crystal diffraction data.

Gas adsorption measurements: CO_2, C_2H_2, and N_2 adsorption isotherms at different temperatures were measured on a Quantachrome Autosorb-iQ instrument under pressures ranging from 0 to 100 kPa. Before each run, about 100 mg of samples were outgassed at 80 °C for 6 h or at 150 °C for 8 h under vacuum to obtain **1a** or **1b**, respectively. Ultrahigh-purity C_2H_2 (99.99%), CO_2 (99.99%), and N_2 (99.99%) were used. Pore size distribution (PSD) data were obtained from the N_2 adsorption isotherm at 77 K based on the nonlocal density functional theory (NLDFT) model.[2]

Breakthrough experiments: The breakthrough experiments were performed at room temperature on a self-made dynamic breakthrough setup as show in Fig. S2. A stainless-steel column (100 mm in length and 6 mm in diameter) was used for sample packing. Before the breakthrough experiment, 200 mg of sample was packed into the column. The flow rate (2 mL/min) of C_2H_2/CO_2 (50:50, v/v) mixture and pressure were controlled by using a pressure-control valve and a mass flow controller. The outlet gas from the column was analyzed using a chromatography with a Porapak Q column (3.15 m in length and 3 mm in diameter) and a thermal conductivity detector (TCD). Helium (23 mL/min) was used as the carrier gas.

Ideal Adsorbed Solution Theory (IAST): In practice, it is difficult to evaluate the gas adsorption selectivity of an adsorbent directly. The co-adsorption or breakthrough measurements are the two main methods. However, the adsorption selectivity of gas mixtures can be predicted effectively by IAST according to the isotherms of single component gases.[3] IAST was first proposed by Myers and Prausnitz[3a], which requires that the adsorption model must be thermodynamic consistent. In this work, IAST was

applied to forecast the adsorption selectivity of C_2H_2/CO_2 binary mixtures. The adsorption selectivity is defined as:[3c]

$$S = \frac{x_1 y_2}{x_2 y_1}$$

where *y* and *x* are the molar fraction in gas phase and adsorbed phase, respectively.

The isosteric heat, Q_{st}: The isosteric heats of C_2H_2 and CO_2 adsorption, Q_{st}, defined as:[4]

$$Q_{st} = RT^2 (\frac{\partial \ln P}{\partial T})$$

were ascertained by the Clausius-Clapeyron equation. The gas adsorption isotherms obtained at 273, 298 and 318 K were fitted by the double Langmuir (DL) equation, respectively.

GCMC Simulation： The adsorption of CO_2 and C_2H_2 in the channels of **1a** or **1b** were calculated by using the Grand-canonical Monte Carlo (GCMC) at 298 K and 100 kPa.[5] The gas molecule and framework were considered to be rigid. The partial charges for carbon and oxygen atoms (CO_2) and carbon and hydrogen atoms (C_2H_2) molecules were 0.576e/-0.288e and 0.281e/-0.281e, respectively,[6] which are similar to the values in reports.[7] The partial charges for atoms of **1a**/**1b** were derived from Q_{Eq} method.[8] The supercell (3 × 3 × 3 unit cell) was used during the simulations. The interaction energies between gas molecule and framework were computed through the Coulomb and Lennard-Jones (LJ) potentials. A cutoff distance of 12.8 Å was used for LJ interactions, and the Coulombic interactions were calculated by using Ewald summation. All parameters for gas molecule and atoms of complex were modeled with the universal forcefield (UFF) embedded in the MS modeling package. For each run, the equilibration and production are performed in 3×10^6 steps, respectively.

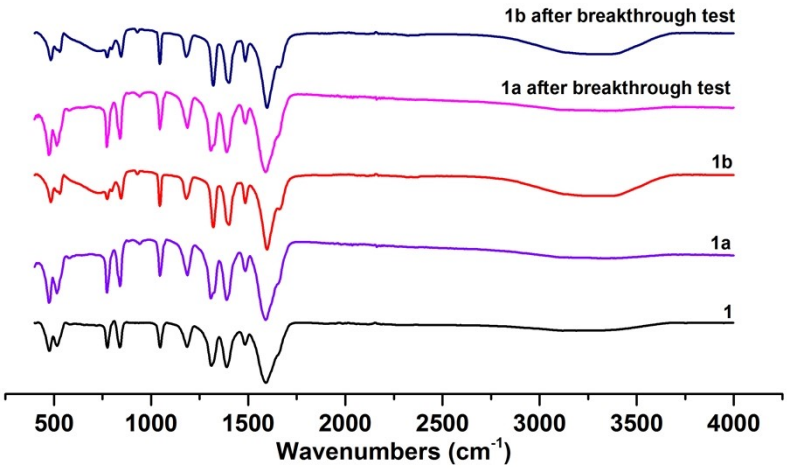

Figure S1. IR spectra of **1, 1a**, and **1b**, and before or after breakthrough test.

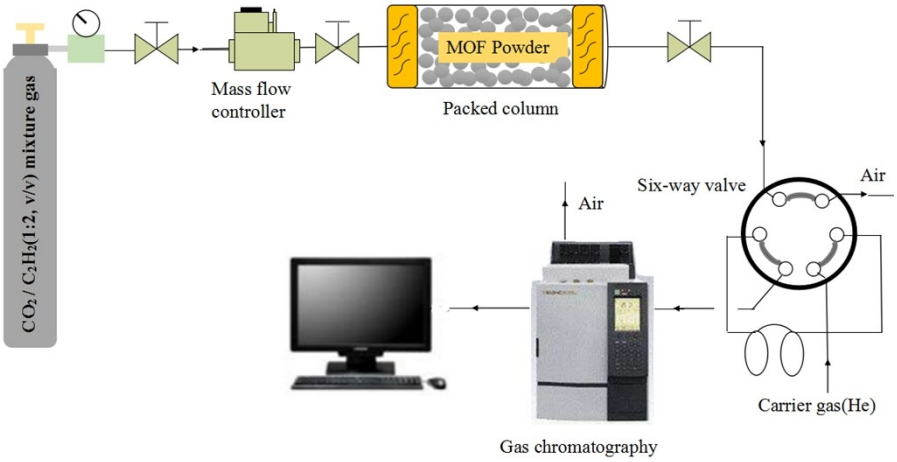

Figure S2. The self-assembly apparatus for breakthrough experiments.

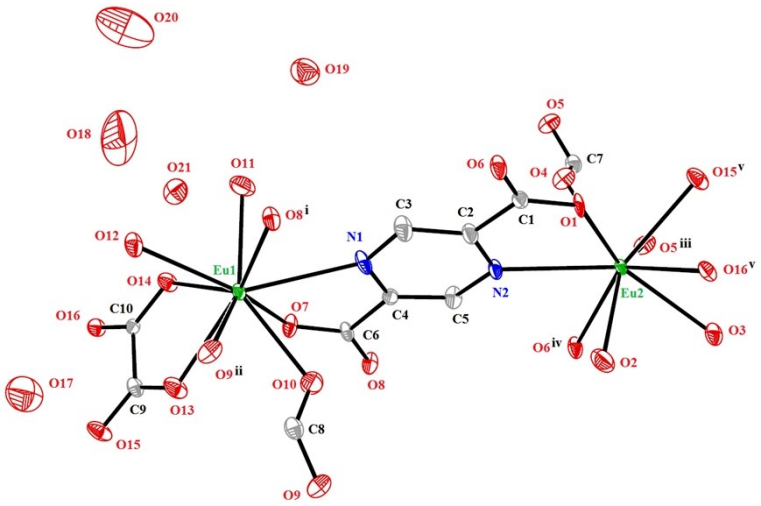

Figure S3. The coordination environment of Eu(III) ions in **1**. All H atoms were omitted for clarity. Symmetry codes: i = x, 1.5-y, 0.5+z; ii = 1-x, 2-y, -z; iii = -x, 1-y, -z; iv = x, 1.5-y, -0.5+z; v = -1+x, 1.5-y, -0.5+z.

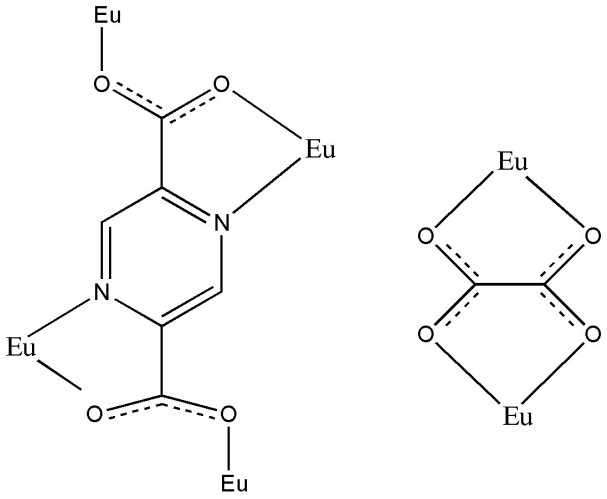

Figure S4 The coordination modes of pzdc and ox ligands in **1**.

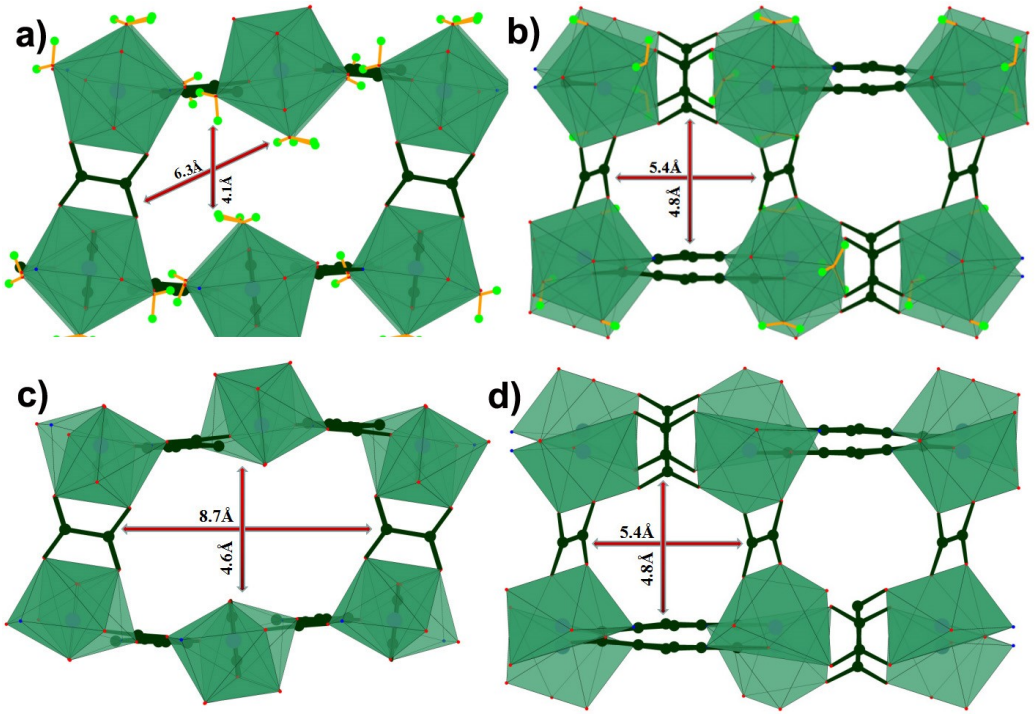

Figure S5. (a, b): View of the pore geometry and aperture sizes of **1a** along the *a* and *c*-axis; (c, d): view of the pore geometry and aperture sizes of **1b** along the *a* and *c*-axis. Color codes: Eu, cyan; O, red; N, blue; H, green.

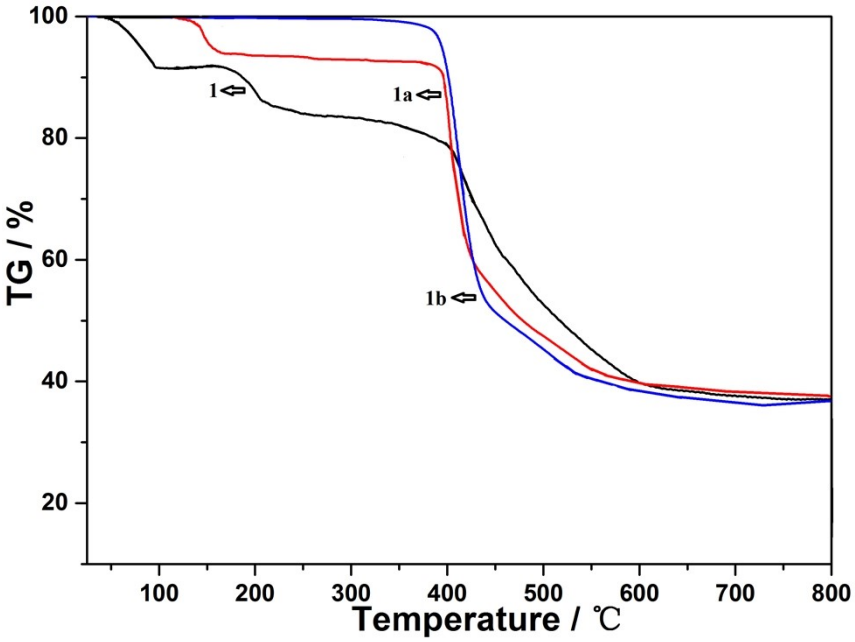

Figure S6. Themogravimetric curves of **1**, **1a** and **1b**.

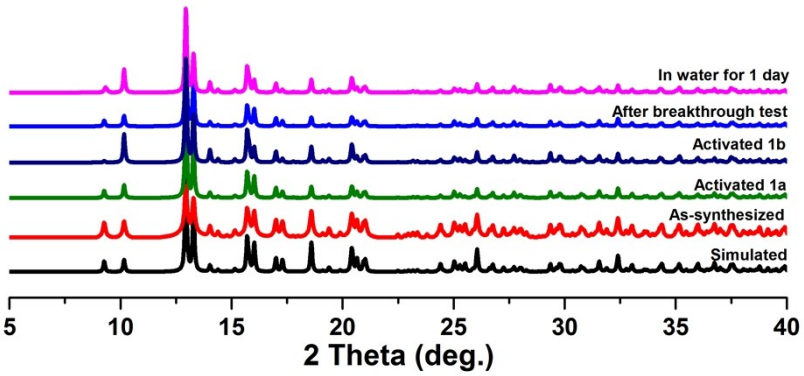

Figure S7. PXRD patterns of **1** samples.

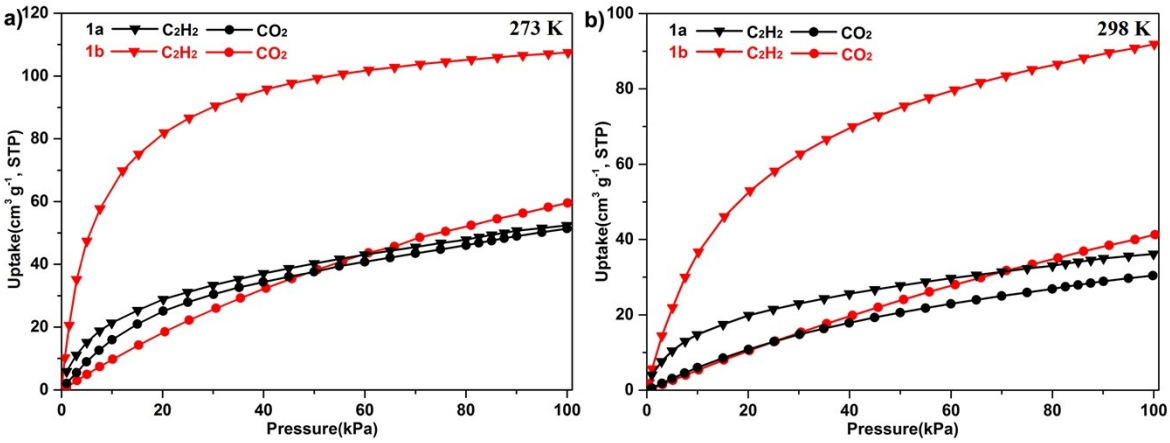

Figure S8. CO_2 and C_2H_2 adsorption isotherms for **1a** and **1b** at 273 K a) and 298 K b), respectively.

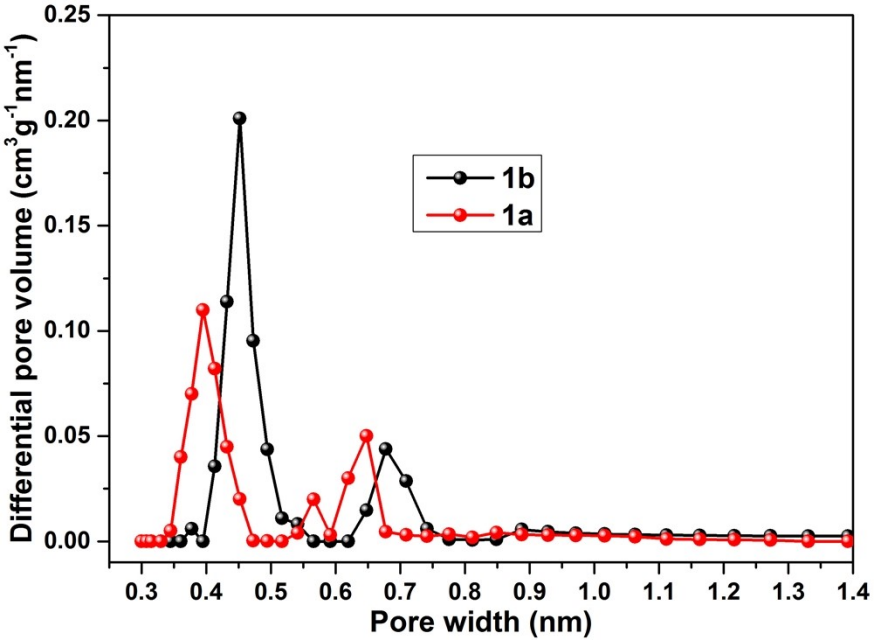

Figure S9. Pore size distribution of **1a** and **1b** based on the NLDFT model.

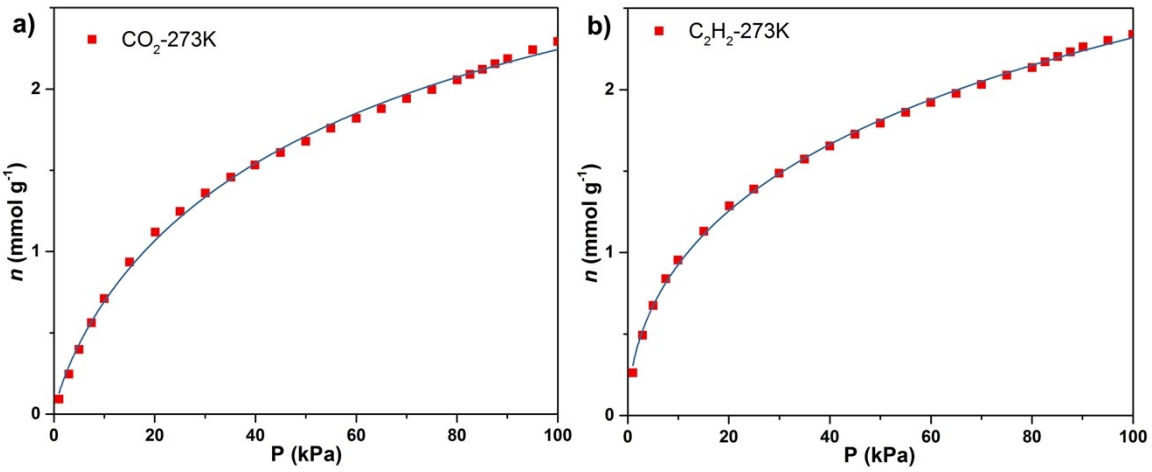

Figure S10. The graphs of the double Langmuir (DL) equation fit for adsorption of CO_2 and C_2H_2 on **1a** at 273 K.

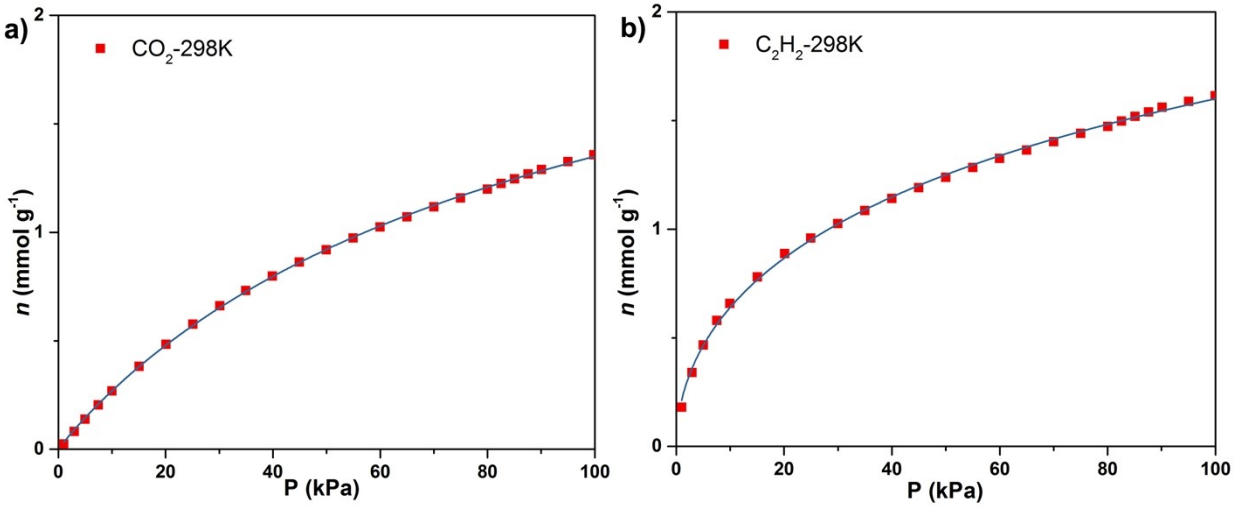

Figure S11. The graphs of the double Langmuir (DL) equation fit for adsorption of CO_2 and C_2H_2 on **1a** at 298 K.

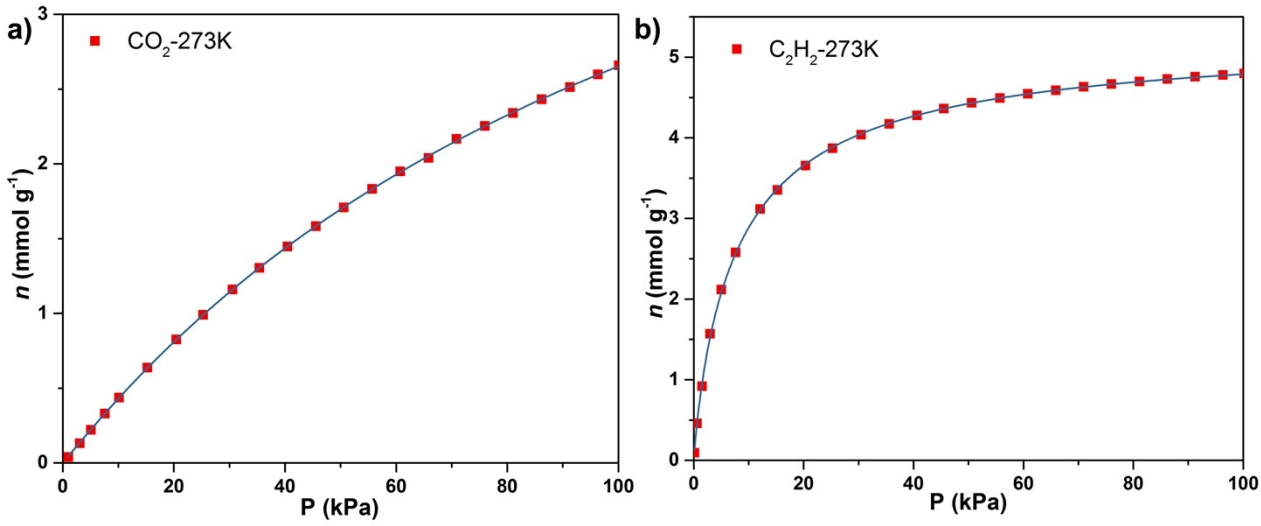

Figure S12. The graphs of the double Langmuir (DL) equation fit for adsorption of CO_2 and C_2H_2 on **1b** at 273 K.

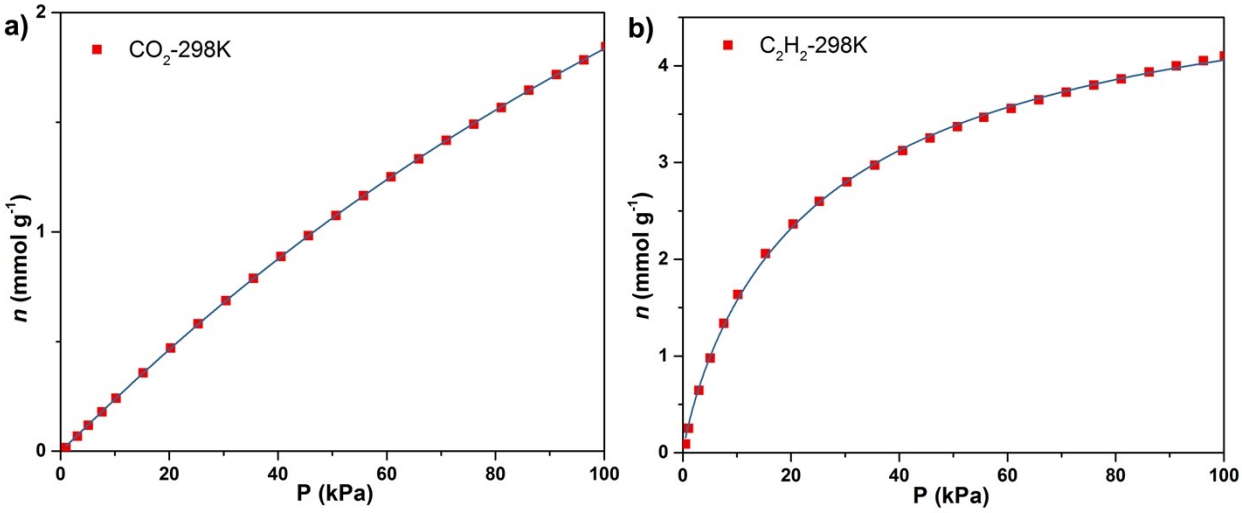

Figure S13. The graphs of the double Langmuir (DL) equation fit for adsorption of CO_2 and C_2H_2 on **1b** at 298 K.

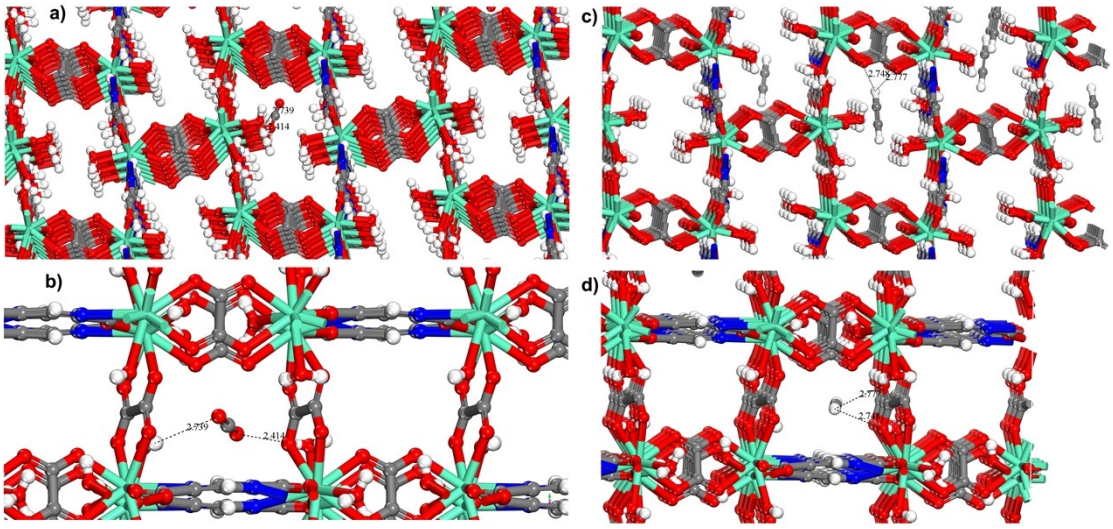

Figure S14. The GCMC derived binding site of CO_2 (a and b) and C_2H_2 (c and d) in the framework of **1a**.

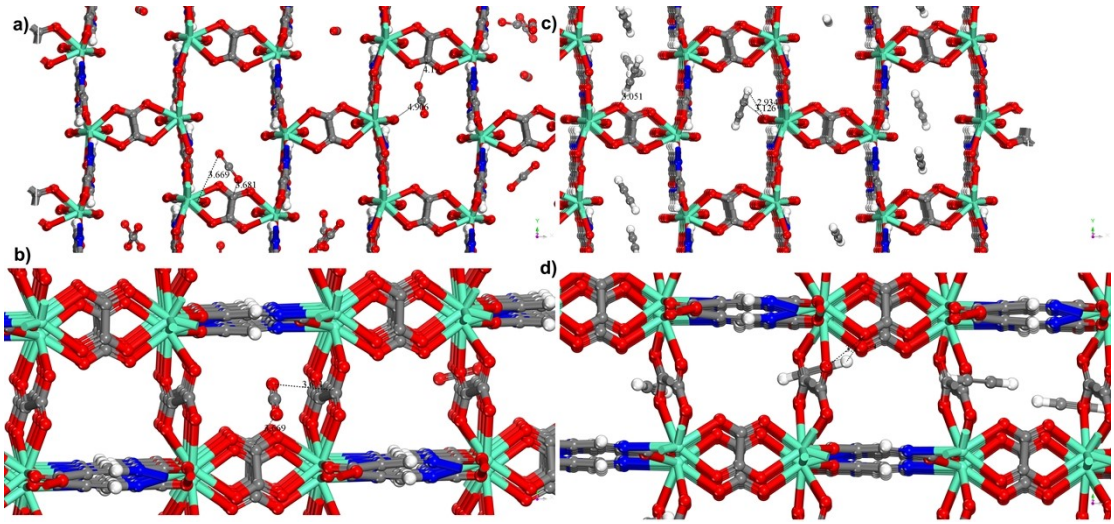

Figure S15. The GCMC derived binding site of CO_2 (a and b) and C_2H_2 (c and d) in the framework of **1b**.

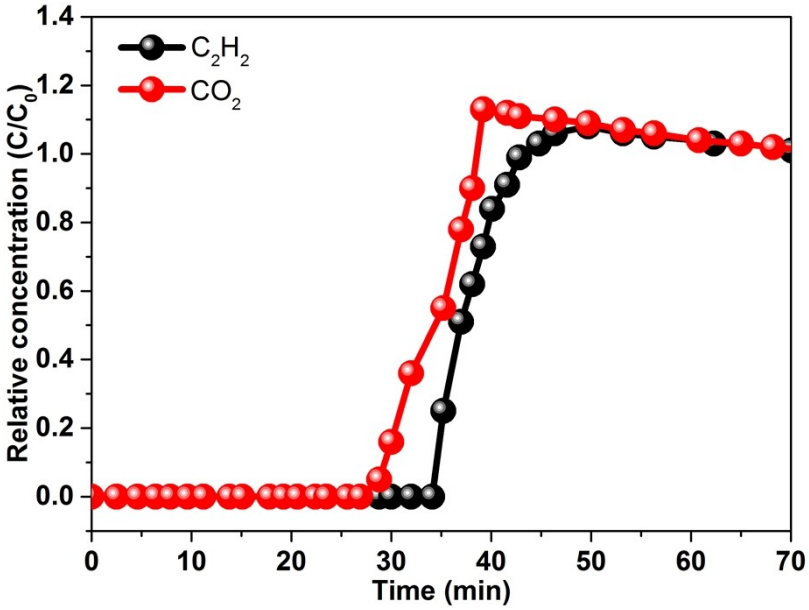

Figure S16. Experimental breakthrough curves of a 50:50 (*v*/*v*) gas mixture of CO_2 and C_2H_2 on **1a** at 298 K and 1.0 bar.

Table S1. Crystallographic data of complex **1**.

Empirical formula	$C_{10}H_{20}O_{21}N_2Eu_2$	Z	4
Formula weight	808.20	D ($Mg.m^3$)	2.398
Temperature (K)	293(2)	μ (mm^{-1})	40.680
Size (mm)	0.08×0.08×0.07	Reflections collected/unique	4007/3079
Crystal system	monoclinic	R_{int}	0.0463
Space group	$P2_1/c$	F(000)	1552
a (Å)	14.5241(4)	θ (°)	3.320-67.250
b (Å)	13.6671(3)	Goodness-of-fit on F^2	1.046
c (Å)	12.3015(4)	$R(I>2\sigma)$	R_1 = 0.0441
α(°)	90		wR_2 = 0.1082
β (°)	113.557(3)		
γ(°)	90	R (all data)	R_1 = 0.0607
			wR_2 = 0.1186
V ($Å^3$)	2238.38(12)	Largest diff. peak and hole ($Å^{-3}$)	1.54, -1.11

$R = \sum(\| F_o \| - \| F_c \|)/\sum \| F_o \|$.
$wR = [\sum w(F_o^2 - F_c^2)^2/\sum w(F_o)^2]^{1/2}$.

Table S2. Selected bond lengths (Å) and bond angles (°) for **1**.

1			
Eu(1)-O(11)	2.414(7)	Eu(1)-N(1)	2.670(7)
Eu(1)-O(13)	2.426(6)	Eu(2)-O(2)	2.403(7)
Eu(1)-O(12)	2.430(6)	Eu(2)-O(1)	2.421(6)
Eu(1)-O(10)	2.430(7)	Eu(2)-O(4)	2.440(6)
Eu(1)-O(7)	2.443(6)	Eu(2)-O(15)^{v}	2.441(6)
Eu(1)-O(8)^{i}	2.445(5)	Eu(2)-N(2)	2.659(6)
O(11)-Eu(1)-O(13)	134.4(2)	O(2)-Eu(2)-O(1)	83.5(2)
O(11)-Eu(1)-O(12)	77.4(2)	O(2)-Eu(2)-O(4)	139.4(2)
O(13)-Eu(1)-O(12)	84.5(2)	O(1)-Eu(2)-O(4)	73.8(2)
O(11)-Eu(1)-O(10)	140.7(2)	O(2)-Eu(2)-O(15)^{v}	135.4(2)
O(11)-Eu(1)-O(14)	68.8(2)	O(2)-Eu(2)-O(3)	80.0(2)
O(13)-Eu(1)-O(14)	65.7(2)	O(1)-Eu(2)-O(3)	140.27(18)
O(12)-Eu(1)-N(1)	142.0(2)	O(2)-Eu(2)-N(2)	74.2(2)

Symmetry codes: i = x, 1.5-y, 0.5+z; v = -1+x, 1.5-y, -0.5+z.

Table S3. Fitting parameters of the Langmuir-Freundlich model for **1a** and **1b**.

	T (K)	**1a**		**1b**	
		C_2H_2	CO_2	C_2H_2	CO_2
q_m	273		86.7588	118.6705	131.8008
	298	98.5253	59.4696	119.8514	134.8220
k	273		0.03448	0.1525	0.00756
	298	0.05054	0.01227	0.0551	0.0038
n	273		0.8009	0.8953	1.0176
	298	0.5271	0.9633	0.8779	1.0312
R^2	273		0.99778	0.99982	0.99997
	298	0.99879	0.99978	0.99945	0.99998

Table S4. The uptakes of CO_2, C_2H_2 and adsorption selectivities of C_2H_2/CO_2 (50:50 CO_2:C_2H_2, *v*/*v*) over reported Ln-MOFs for selective adsorption of C_2H_2 over CO_2.

Adsorbents	*T* (K)	*P* (kPa)	CO_2 uptake ($cm^3\ g^{-1}$)[a]	C_2H_2 uptake ($cm^3\ g^{-1}$)[a]	Selectivity (IAST)[b]	*Ref.*
UPC-80	298	100	39.23	77.28	6.34	7
JXNU-5	298	100	34.80	55.9	9.0	7
JXNU-10	298	100	24.00	53.3	2.68	8
1-Eu	298	100	62.3	109.2	4.1	9
UTSA-222	298	100	42.70	85.3	4.6	10
BUT-70B	298	100	10.69	81.7	8.5	11
1a	298	100	30.39	36.15	3.2	this work
1b	298	100	41.20	91.84	12.7	this work

[a] Gravimetric uptake ($cm^3\ g^{-1}$) at 100 kPa. [b] Selectivity calculated from IAST for the C_2H_2/CO_2 (50:50, *v*/*v*) mixture at 100 kPa.

Table S5. Comparison of breakthrough experiments parameters of SIFSIX-3-Ni, CD-MOF-1, CD-MOF-2 and **1a**.

Adsorbents	T (K)	Sample weight (mg)	Total flow (mL min^{-1})	C_2H_2/CO_2 mixture	Breakthrough time (min)	Selectivity (IAST)	*Ref.*
UPC-80	298	unspecified	2.0	50:50, *v/v*	15.8	6.34	13a
JXNU-5	298	460	2.0	50:50, *v/v*	14.0	9.0	13b
JXNU-10	298	unspecified	2.0	50:50, *v/v*	26.1	2.68	13c
1-Eu	298	655.9	2.0	50:50, *v/v*	27.3	4.1	13f
1b	298	200	2.0	50:50, *v/v*	28.8	12.72	this work

References

[1] (a) Bruker. APEX II Software, version 6.3.1; Bruker AXS Inc: Madison, Wisconsin, USA, 2004; (b) G. M. Sheldrick, A short history of SHELX. *Acta Crystallogr., Sect. A*, 2008, **64**, 112−122; (c) V. A. Blatov, A. P. Shevchenko, D. M. Proserpio, *Cryst. Growth Des.*, 2014, **14**, 3576−3586; (d) G. Nandi, R. Thakuria, H. M. Titi, R. Patra, I. Goldberg, *CrystEngComm*, 2014, **16**, 5244−5256.

[2] Y. Zhu, S. Murali, M. D. Stoller, K. J. Ganesh, W. Cai, P. J. Ferreira, A. Pirkle, R. M. Wallace, K. A. Cychosz, M. Thommes, D. Su, E. A. Stach, R. S. Ruoff, *Science*, 2011, **332**, 1537-1541.

[3] (a) A.L. Myers, J.M. Prausnitz, *AIChE J.*,1965, **11**, 121-127; (b) K. Sumida, D.L. Rogow, J.A. Mason, T.M. McDonald, E.D. Bloch, Z.R. Herm, T.H. Bae, J.R. Long, *Chem. Rev.*, 2012, **112**, 724-781; (c) Y. Chen, D. Lv, J. Wu, J. Xiao, H. Xi, Q. Xia, Z. Li, *Chem. Eng. J.*, 2017, **308**, 1065-1072; (d) F.A. Kloutse, A. Hourri, S. Natarajan, P. Benard, R. Chahine, *Sep. Purif. Technol.*, 2018, **197**, 228-236; (e) F.A. Kloutse, A. Hourri, S. Natarajan, P. Benard, R. Chahine, *Micropor. Mesopro. Mater.*, 2018, **271**, 175-185.

[4] (a) L. Zhang, K. Jiang, Y. Yang, Y. Cui, B. Chen, G. Qian, *J. Solid State Chem.*, 2017, **255**, 102-107; (b) H. Pan, J.A. Ritter, P.B. Balbuena, *Langmuir*, 1998, **14**, 6323-6327; (c) A. F. Kloutse, R. Zacharia, D. Cossement, R. Chahine, R. Balderas-Xicohtencatl, H. Oh, B. Streppel, M. Schlichtenmayer, M. Hirsche, *Appl. Phys. A*, 2015, **121**, 1417-1424.

[5] (a) J. P. Perdew, Y. Wang, *Phys. Rev. B*, 1992, **45**, 13244-13249; (b) D. Wu, C. Wang, B. Liu, Q. Yang, C. Zhong, *AIChE J.*, 2012, **58**, 2078-2084; (c) Sorption, v. Accelrys, Inc, San Diego, 2005.

[6] (a) A. Hirotani, K. Mizukami, R. Miura, H. Takaba, T. Miya, A. Fahmi, A. Stirling, M. Kubo and A. Miyamoto, *Appl. Surf. Sci.*, 1997, **120**, 81; (b) H.-H. Wang, W.-J. Shi, L. Hou, G.-P. Li, Z. Zhu and Y.-Y. Wang, *Chem. Eur. J.*, 2015, **21**, 16525.

[7] (a) J. Yu and P. B. Balbuena, *J. Chem. Phys. C*, 2013, **117**, 3383; (b) R. Vaidhyanathan, S. S. Iremonger, G. K. H. Shimizu, P. G. Boyd, S. Alavi and T. K. Woo, *Angew. Chem. Int. Ed.*, 2012, **51**, 1826.

[8] H. Y. Yang, Y. Z. Li, W. J. Shi, L. Hou, Y. Y. Wang, Z. Zhu, *Dalton Trans.*, 2017, **46**, 11722-11727